

Semantic-guided Image Virtual Attribute Learning for Noisy Multi-label Chest X-ray Classification

Yuanhong Chen¹ * Fengbei Liu¹ * Yu Tian¹ Yuyuan Liu¹
Gustavo Carneiro¹

Australian Institute for Machine Learning, University of Adelaide

Abstract. Deep learning methods have shown outstanding classification accuracy in medical image analysis problems, which is largely attributed to the availability of large datasets manually annotated with clean labels. However, such manual annotation can be expensive to obtain for large datasets, so we may rely on machine-generated noisy labels. Many Chest X-ray (CXR) classifiers are modelled from datasets with machine-generated labels, but their training procedure is in general not robust to the presence of noisy-label samples and can overfit those samples to produce sub-optimal solutions. Furthermore, CXR datasets are mostly multi-label, so current noisy-label learning methods designed for multi-class problems cannot be easily adapted. To address such noisy multi-label CXR learning problem, we propose a new learning method based on estimating image virtual attributes using semantic information from the label to assist in the identification and correction of noisy multi-labels from training samples. Our experiments on diverse noisy multi-label training sets and clean testing sets show that our model has state-of-the-art accuracy and robustness across all datasets.

Keywords: Multi-label learning · Multi-modal learning · Noisy-label learning · Chest X-ray.

1 Introduction

The promising results produced by deep neural networks (DNN) in medical image analysis (MIA) problems [16] is generally attributed to the availability of large datasets with accurately annotated labels. Given the high cost of acquiring such datasets, the field has resorted to a more affordable automatic annotation by Natural Language Processing (NLP) approaches that extract multiple image labels (each label representing a disease) from radiology reports [10, 25]. However, mistakes made by NLP combined with uncertain findings from the reports can introduce labelling mistakes. Recent research [20, 21] suggests that existing NLP-annotated large-scale Chest X-ray (CXR) datasets [10, 25] contain noisy multi-labels that can mislead the supervised training process.

* First two authors contributed equally to this work.

Current CXR multi-label classification methods [1, 7, 19, 23] show promising results, even without addressing this noisy multi-label problem. Rajpurkar et al. [23] develop a DNN to automatically detect pneumonia from CXR images. Ma et al. [19] introduce a new cross-attention network to extract meaningful representations. Hermoza et al. [7] propose a weakly-supervised method to diagnose and localise diseases. Although these methods show accurate multi-label classifications, there is still potential for improvement that can be realised by properly addressing the noisy multi-label learning problem present in CXR datasets [10, 25].

Learning with noisy label (LNL) on computer vision tasks can be divided into two frameworks. *Noise-cleaning* methods aim to identify noisy samples from a multi-class training set. Han et al. [6] propose to train two models and identify noisy samples from prediction differences by the two networks. Huang et al. [9] identify noisy samples by switching learning rate and selecting samples with unstable prediction. DivideMix [15] is the current state-of-the-art (SOTA) LNL that un-labels samples classified as noisy label and runs a semi-supervised learning method. However, given that most large-scale CXR datasets are multi-label, the methods above would be useful if we could perform not only sample-wise, but also label-wise noise-cleaning, which is challenging. Another type of LNL approach is based on *label transition matrix estimation* for multi-class problems. Goldberger et al. [5] propose a noise adaptation layer to estimate the label transition matrix using a few clean samples. Yao et al. [27] reduce the transition matrix estimation error by introducing an intermediate class and a factorised transition matrix. Xia et al. [26] estimate part-dependent transition matrix for complex noise conditions. Although effective in noisy multi-class problems, these methods are challenging to be adapted to a noisy multi-label scenario because the label correlation between multiple labels will also influence the noisy label generation, making the estimation of the label transition matrix much harder.

In this paper, we propose a new method to learn with noisy multi-label when training a CXR classifier, named Semantic Guided Virtual Attribute Learning (SGVAL). The main innovation of SGVAL is the exploration of multi-modal semantic information to estimate image virtual attributes that are then used to identify and correct noisy multi-labels from training images. The main technical contributions of our new noisy multi-label learning approach SGVAL are:

- A new method that extracts multiple virtual image attributes of an image using a loss that ranks the semantic vectors (represented by word embeddings from BioBERT [14]) that represent the diseases in the training image labels. We build a new noisy-label sample classifier based on these learned attributes and semantic vectors;
- A new graph representation, where nodes denote virtual image attributes and edge weights represent the similarity between nodes, and this graph is used to re-label the samples classified as noisy from above.

We show the effectiveness of our approach using a new benchmark that consists of training with two large-scale noisy multi-label CXR datasets and testing on two clean multi-label CXR datasets. Results show that our approach has more

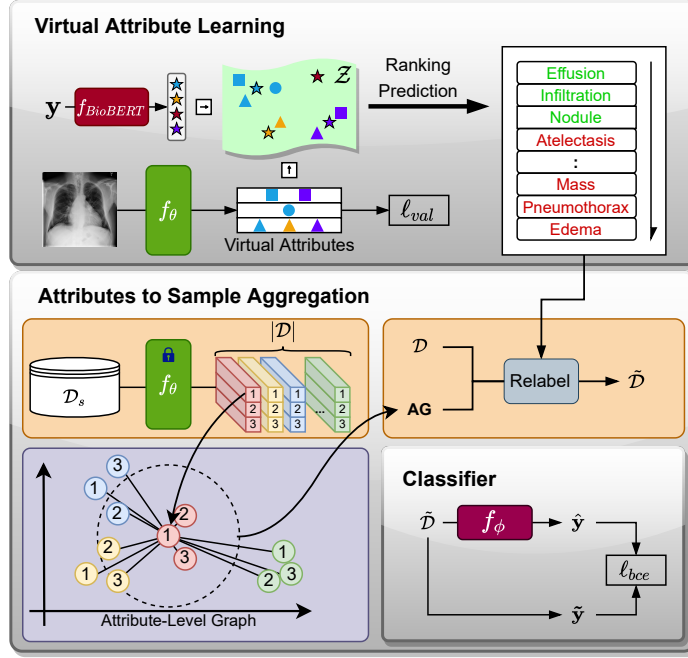


Fig. 1. SGVAL. The **virtual attribute learning (VAL)** module estimates multiple attributes for each image, which are learned using the semantic information provided by BioBERT [14] (represented by word embeddings from the image label \mathbf{y}) in the semantic space \mathcal{Z} . In the figure, the output from BioBERT is represented by stars, where colours represent labels, and the virtual attributes are represented by squares, circles and triangles in \mathcal{Z} , each representing a different feature of image, with colours indicating labels. VAL learns the attributes with ℓ_{val} by ranking the semantic vectors representing the training image labels. VAL also classifies the training samples into clean or noisy by verifying if the top-ranked labels from the image coincides with the training labels. The **attributes to sample (A2S) aggregation** builds an attribute-level graph using all attributes from all training images, which is then used to re-label noisy training samples (from VAL) with a K nearest neighbor classification to form $\tilde{\mathcal{D}}$. The classifier f_ϕ is trained with the re-labelled dataset $\tilde{\mathcal{D}}$.

accurate classifications on clean testing sets than previous multi-label classifiers developed for CXR datasets and noisy-label classifiers developed for computer vision multi-class tasks.

2 Method

We assume the availability of a noisy multi-label CXR training data denoted by $\mathcal{D} = \{\mathbf{x}_i, \mathbf{y}_i\}_{i=1}^{|\mathcal{D}|}$, where $\mathbf{x}_i \in \mathcal{X} \subset \mathbb{R}^{H \times W \times R}$ represents an image of size $H \times W$ and R colour channels, $\mathbf{y}_i \in \mathcal{Y} = \{0, 1\}^{|\mathcal{C}|}$ denotes the multiple labels with each class being present “1” or not “0”. The testing set is similarly defined.

2.1 Semantic Guided Virtual Attribute Learning (SGVAL)

Our proposed SGVAL is a noisy multi-label learning approach that aims to correct the mislabelled samples with an estimated soft pseudo-label. The proposed SGVAL, depicted in Fig. 1, contains two major processes, namely: 1) a virtual attribute learning process that transforms a training sample from the image space into multiple virtual attributes in the semantic space \mathcal{Z} populated by word embeddings of image labels formed by BioBERT [14], and 2) an attribute to sample aggregation module that builds an attribute-level graph to re-label the training data. The final objective of SGVAL is to train a model $\hat{\mathbf{y}} = f_\phi(\mathbf{x})$ with the binary cross entropy loss (BCE), with $\hat{\mathbf{y}} \in [0, 1]^{|C|}$, as follows:

$$\phi^* = \arg \min_{\phi} \frac{1}{|\tilde{\mathcal{D}}|} \sum_{(\mathbf{x}_i, \tilde{\mathbf{y}}_i) \in \tilde{\mathcal{D}}} \ell_{bce}(\tilde{\mathbf{y}}_i, f_\phi(\mathbf{x}_i)), \quad (1)$$

where $\ell_{bce}(\tilde{\mathbf{y}}_i, f_\phi(\mathbf{x}_i)) = -(\tilde{\mathbf{y}}_i \log f_\phi(\mathbf{x}_i)) + (1 - \tilde{\mathbf{y}}_i) \log(1 - f_\phi(\mathbf{x}_i))$, and $\tilde{\mathcal{D}}$ has the same images as \mathcal{D} , but with updated labels $\tilde{\mathbf{y}}$. Below, we explain the two components of SGVAL.

2.2 Virtual Attribute Learning (VAL)

VAL trains a model to output the virtual attribute matrix from an input image, as in $\mathbf{V} = f_\theta(\mathbf{x})$. The matrix $\mathbf{V} = [\mathbf{v}(1), \dots, \mathbf{v}(M)]^\top \in \mathbb{R}^{M \times Z}$ contains M virtual attributes $\mathbf{v}(m) \in \mathcal{Z} \subset \mathbb{R}^Z$ trained to rank the semantic label information, represented by the word embeddings of the diseases in \mathcal{C} . We use BioBERT [14], a medical domain language representation model pre-trained on biomedical corpora to extract meaningful semantic information for all the diseases, to produce these word embeddings, as follows: $\mathbf{w}(c) = f_{BioBERT}(\mathbf{y}(c) = 1)$, where $\mathbf{w}(c) \in \mathcal{Z}$, forming the matrix $\mathbf{W} = [\mathbf{w}(1), \dots, \mathbf{w}(|\mathcal{C}|)]^\top \in \mathbb{R}^{|\mathcal{C}| \times Z}$ that represents the word embeddings for all $|\mathcal{C}|$ labels. VAL is trained with:

$$\theta^* = \arg \min_{\theta} \frac{1}{|\mathcal{D}|} \sum_{(\mathbf{x}_i, \mathbf{y}_i) \in \mathcal{D}} \omega_i \ell_{val}(\mathbf{x}_i, \mathbf{y}_i, \theta) + \beta \ell_{reg}(\mathbf{x}_i, \theta) \quad (2)$$

where $\omega_i = \left(\left(\sum_{c=1}^{|\mathcal{C}|} \mathbb{I}(\mathbf{y}_i(c) = 1) \right) \times \left(\sum_{c=1}^{|\mathcal{C}|} \mathbb{I}(\mathbf{y}_i(c) = 0) \right) \right)^{-1}$ is a normalisation that controls the ranking weight based on the number of positive and negative labels ($\mathbb{I}(\cdot)$ represents an indicator function) [2, 28], and the hyper-parameter β weights the regulariser. The loss functions ℓ_{val} and ℓ_{reg} in (2) are defined as:

$$\begin{aligned} \ell_{val}(\mathbf{x}_i, \mathbf{y}_i, \theta) = & \sum_{\substack{\mathbf{w}(p) \in \mathbf{W}, \\ \mathbf{y}_i(p)=1}} \sum_{\substack{\mathbf{w}(n) \in \mathbf{W}, \\ \mathbf{y}_i(n)=0}} \log \left(1 + \exp \left(\max_{\mathbf{v} \in \mathbf{V}_i} (\langle \mathbf{v}, \mathbf{w}(n) \rangle) - \max_{\mathbf{v} \in \mathbf{V}_i} (\langle \mathbf{v}, \mathbf{w}(p) \rangle) \right) \right), \end{aligned} \quad (3)$$

with \mathbf{W} denoting the word embeddings for the $|\mathcal{C}|$ labels, $\langle \cdot, \cdot \rangle$ representing the dot product operator, $\mathbf{V}_i = f_\theta(\mathbf{x}_i)$, and ℓ_{reg} reduces the variance of each attribute with

$$\ell_{reg}(\mathbf{x}_i, \theta) = \sum_{\mathbf{v}(m) \in \mathbf{V}_i} \frac{(\mathbf{v}(m) - \bar{\mathbf{v}}(m))^\top (\mathbf{v}(m) - \bar{\mathbf{v}}(m))}{Z - 1}, \quad (4)$$

where $\bar{\mathbf{v}}(m) = \frac{\mathbf{1}_Z^\top \mathbf{v}(m)}{Z}$ ($\mathbf{1}_Z$ denotes a vector of Z ones). The loss $\ell_{val}(\cdot)$ defined in (3) is inspired by previous multi-label learning methods [28], which learns a single attribute to ensure that the dot product $\langle \mathbf{v}, \mathbf{w}(p) \rangle$ ranks ahead of the $\langle \mathbf{v}, \mathbf{w}(n) \rangle$. Differently from [28], we replace this single attribute by M attributes to account for the fact that CXR images contain multiple labels with distinct semantic meanings (e.g., "fracture" and "cardiomegaly"). Hence, the learned M virtual attributes have a better chance to more comprehensively describe the training sample, where M is proportional to the complexity of the dataset.

2.3 Attributes to Sample Aggregation (A2S)

A2S re-labels the training data to form $\tilde{\mathcal{D}} = f_{A2S}(f_\theta(\mathbf{x}), \mathcal{D})$, which updates the training set by first classifying the samples as clean and noisy, and then by re-labelling the noisy ones using a graph-based approach that uses the learned attributes. The classification of training samples into clean or noisy verifies if the top-ranked labels from the image \mathbf{x}_i , represented by $\arg \text{sort}_{\mathbf{w} \in \mathbf{W}} \max_{\mathbf{v} \in \mathbf{V}_i} (\langle \mathbf{v}, \mathbf{w} \rangle)$ coincides with the label \mathbf{y}_i annotated with "1", where $\mathbf{V}_i = f_\theta(\mathbf{x}_i)$ from (3). In the affirmative case, we classify the sample as clean-label and keep the original label. For the samples outside of the clean-label set, they are considered to have at least one noisy-label, and need to be re-labelled, as described below¹.

Attribute-level Graph (AG) To re-label noisy-label training samples, we first build the AG with the learned attributes as graph nodes and their similarity as edge weights. More specifically, each training image $i \in \{1, \dots, |\mathcal{D}|\}$ is represented by M nodes formed by $[\mathbf{v}_i(1), \dots, \mathbf{v}_i(M)]^\top$ that are the rows of $\mathbf{V}_i = f_\theta(\mathbf{x}_i)$, and the edge weight between the m^{th} attribute of the i^{th} image and the n^{th} attribute of the j^{th} image is defined by $e(\mathbf{v}_i(m), \mathbf{v}_j(n)) = 1/\|\mathbf{v}_i(m) - \mathbf{v}_j(n)\|_2$. This means that the graph has the set of nodes denoted by $\mathcal{V} = \{\mathbf{v}_i(m)\}_{i=1, m=1}^{|\mathcal{D}|, M}$ and edges $\mathcal{E} = \{e(\mathbf{v}_i(m), \mathbf{v}_j(n))\}_{i,j=1, m,n=1}^{|\mathcal{D}|, M}$.

Attribute-graph Based Re-labeling We find the K nearest neighbouring training images to image i with using the AG nodes, as in:

$$\mathcal{N}_K(\mathbf{V}_i) = \text{top}K_{m \in \{1, \dots, M\}, \mathbf{v}_j(n) \in \mathcal{V}}(e(\mathbf{v}_i(m), \mathbf{v}_j(n))), \quad (5)$$

where $\text{top}K_{m \in \{1, \dots, M\}, \mathbf{v}_j(n) \in \mathcal{V}}(\cdot)$ returns the unique image indices from the K nodes with the largest edge weights.

¹ See supplementary material for pseudo-code.

For all samples identified as noisy-label, we update their labels with:

$$\tilde{\mathbf{y}}_i = \lambda \times \mathbf{y}_i + (1 - \lambda) \times \min \left(\mathbf{1}_{|\mathcal{C}|}, \sum_{j \in \mathcal{N}_K(\mathbf{V}_i)} \mathbf{y}_j \right), \quad (6)$$

which is a convex combination, parameterised by λ , of the original label \mathbf{y}_i and the labels of the training images from $\mathcal{N}_K(\mathbf{V}_i)$ in (5).

3 Experiments

For the experiments, we use the datasets listed below.

Noisy Training Sets. The *NIH Chest X-ray14* [25] contains 112,120 frontal-view CXR images from 30,805 different patients labelled with 14 disease classes. The dataset is created to study multi-label problem, where each image can have between 0 and 14 annotated pathologies. The original training set [25] is used for all the experiments which contains 86,524 images with a maximum of 9 labels per image. The *CheXpert (CXP)* dataset consists of 224,316 frontal-view chest radiographs of 65,240 patients labelled for the presence of 14 common chest radiographic observations. We use the original training set [11] which contains 1,559,031 images with a maximum of 8 labels per image. The labels of these two datasets are obtained from an NLP algorithm, which contaminates the training sets with label noise [20].

Clean Testing Sets. The *OpenI* [4] dataset contains 3,999 radiology reports and 7,470 frontal/lateral-view chest X-ray images from the Indiana Network for Patient Care. We use all frontal-views images for evaluation resulting a total number of 3,818 images and 19 manually annotated diseases. We also use the large-scale dataset *PadChest* [3], which contains 158,626 images with 27 chest radiographic observations. PadChest have a mixture of machine labelled and manually labelled annotation, but we only use the manually labelled annotations (about 37.5% of total images) for all the experiments.

Data Pre-processing Due to the inconsistency of total number of observations for each dataset, we trim the original datasets and only keep those samples that contain labels present in all datasets. Please see the statistics of the final dataset in the supplementary material.

3.1 Implementation Details

We resize the NIH ChestX-ray14 [25] training images to 512×512 , CheXpert [11] to 256×256 and images are normalised using ImageNet [24] mean and standard deviation. We use random resize crop and random horizontal flipping as data augmentation. The BioBERT word embeddings in \mathbf{W} are L2 normalised. For the VAL model $f_\theta(\cdot)$, we use DenseNet121 [8], initialized with ImageNet [24] pre-trained weights, which is trained with Adam optimiser [13] using a learning rate of 0.0001 with cosine annealing decay [18], batch size of 16 images and 30 epochs. The attribute graph is implemented with the Faiss [12] library for

Table 1. Class-level testing AUC results for models **trained on NIH**. Best results for OpenI/PadChest are in **red/blue**.

Models	ChestXNet [23]		Renato et al [7]		DivideMix [15]		CAN [19]		SGVAL	
Datasets	OpenI PadChest		OpenI PadChest		OpenI PadChest		OpenI PadChest		OpenI PadChest	
Atelectasis	86.97	84.99	86.85	83.59	70.98	73.48	84.83	79.88	87.00	84.93
Cardiomegaly	89.89	92.50	89.49	91.25	74.74	81.63	90.87	91.72	91.68	92.45
Effusion	94.38	96.38	95.05	96.27	84.49	97.75	94.37	96.29	95.00	96.52
Infiltration	76.72	70.18	77.48	64.61	84.03	81.61	71.88	73.78	81.68	76.93
Mass	53.65	75.21	95.72	86.93	71.31	77.41	87.47	85.81	95.27	86.76
Nodule	86.34	75.39	82.68	75.99	57.45	63.89	69.71	68.14	85.15	75.59
Pneumonia	91.44	76.20	88.15	75.73	64.65	72.32	84.79	76.49	89.87	77.61
Pneumothorax	80.48	79.63	75.34	74.55	71.56	75.46	82.21	79.73	84.02	80.17
Edema	83.73	98.07	85.31	97.78	80.71	91.81	82.75	96.41	85.85	98.21
Emphysema	82.37	79.10	83.26	79.81	54.81	59.91	79.38	75.11	85.43	81.71
Fibrosis	90.53	96.13	86.93	96.46	76.96	84.71	83.17	93.20	92.60	96.52
Pleural Thicken	81.58	72.29	77.99	69.95	63.98	58.25	77.59	67.87	86.00	73.11
Hernia	89.82	86.72	93.90	89.29	66.34	72.11	87.37	86.87	95.48	93.15
Mean AUC	83.68	83.29	86.01	83.25	70.92	76.18	82.80	82.41	88.85	85.67

Table 2. Class-level testing AUC results for models that **trained on CheXpert**. Best results for OpenI/PadChest are in **red/blue**.

Models	ChestXNet [23]		Renato et al [7]		DivideMix [15]		CAN [19]		SGVAL	
Datasets	OpenI PadChest		OpenI PadChest		OpenI PadChest		OpenI PadChest		OpenI PadChest	
Cardiomegaly	84.00	80.00	87.01	87.20	71.14	66.51	82.83	85.89	92.50	92.86
Edema	88.16	98.80	87.92	98.72	75.36	95.51	86.46	97.47	86.97	95.33
Pneumonia	65.82	58.96	65.56	53.42	57.65	40.53	61.88	54.83	66.67	62.13
Atelectasis	77.70	72.23	78.40	75.33	73.65	64.12	80.13	72.87	82.10	74.49
Pneumothorax	77.35	84.75	62.09	78.65	68.75	54.05	51.08	71.57	68.36	76.92
Effusion	85.81	91.84	87.00	93.94	78.60	79.89	88.43	92.92	88.79	93.85
Fracture	57.64	60.26	57.47	53.77	60.35	59.43	59.92	60.44	65.04	64.98
Mean AUC	76.64	78.12	75.06	77.29	69.36	65.72	72.96	76.57	78.63	80.08

efficient similarity search with Euclidean distance. The search process in (5) takes 5 seconds for all training samples from NIH. For the classifier $f_\phi(\cdot)$, we use another DenseNet121 [8], initialized with ImageNet [24] pre-trained weights. We train $f_\phi(\cdot)$ with Adam optimiser [13] using a learning rate of 0.05, batch size of 16 images and 30 epochs. We empirically set the multi-step learning rate decay at 23 and 27 epochs with a decay rate of 0.1. The classification results are assessed with the area under the receiver operating characteristic curve (AUC-ROC) for each class and the mean over all available disease classes, following previous works [7, 17, 23]. All experiments are implemented with Pytorch [22] and conducted on an NVIDIA RTX3090 GPU (24GB). Training takes 23h for NIH and 15h for CheXpert. Testing for a single image takes 13.41ms for NIH and 12.24ms for CheXpert.

Table 3. Ablation study of our method on NIH for mixup coefficient (6), number of attributes M from Sec. 2.2 and label smoothing. Best results per column are highlighted

Experiments	Mixup Coefficient			Number of Attributes			Label smoothing		
Settings	λ	OpenI	PadChest	M	OpenI	PadChest	ϵ	OpenI	PadChest
AUC	0.1	87.37	85.26	1	87.25	84.53	0.1	82.69	81.64
	0.3	88.31	85.05	3	88.85	85.67	0.3	79.54	81.42
	0.5	87.17	85.35	5	86.55	84.36	-	-	-
	0.7	88.85	85.67	7	87.06	85.26	-	-	-
	0.9	86.91	84.79	9	87.28	84.56	-	-	-

3.2 Results

Tab. 1 shows the testing AUC results of the learning with NIH [25] training set and testing on OpenI [4] and PadChest [3]. Our model surpasses the second best method [7] by 2.84% and 2.42% on the two test sets. We also report testing performance on OpenI [4] and PadChest [3] based on the model trained on CheXpert [11] in Tab. 2. Our model surpasses the second best result [23] by 1.99% and 1.96% on the two test sets. We notice that there is large gap between the model performance on certain classes between Tab. 1 and Tab. 2. For our model, we see 23.2% and 15.48% gaps for *Pneumonia* on OpenI [4] and PadChest [3], respectively. We speculate that this is due to the lower image quality of CheXpert.

3.3 Ablation Study

Table 3 shows a study of two important hyper-parameters of our SGVAL model: label mixup coefficient λ for (6), and the number of attributes M from Sec. 2.2. We test five evenly spaced numbers, as in $\lambda \in \{0.1, 0.3, 0.5, 0.7, 0.9\}$ and $M \in \{1, 3, 5, 7, 9\}$. The label mixup coefficient λ controls the contribution of pseudo-labels from sample-level graph, and we fix number of attributes $M = 3$ for this experiment. We show that when $\lambda = 0.7$ the model achieves the best results, while relying too much on the pseudo-labels from sample-level graph ($\lambda = 0.1$) or the original noisy labels ($\lambda = 0.9$) worsens the performance. We also report the results for a varying the number of attributes M , where we fix $\lambda = 0.7$. We find that $M = 3$ reaches the best results, and there is no improvement for a larger number of attributes. One can argue that the label smoothing in the re-labeling of (6) is the main reason for improving the results, so we show the performance of a training that smooths the training labels by reducing the positive class labels to $1 - \epsilon$ and increasing the negative class to ϵ . The results show that our method outperforms the best model for label smoothing with $\epsilon = 0.1$ by 6.16% and 4.03% on OpenI [4] and PadChest [3], demonstrating the effectiveness of the our SGVAL.

4 Conclusion and Future Work

In this paper, we proposed SGVAL, a new method to learn with noisy multi-label when training a CXR image classifier. SGVAL explores the multi-modal semantic information, represented by word embeddings from BioBert [14], to estimate image virtual attributes which is used to find noisy multi-label training samples. We then use the estimated image virtual attributes to form a graph representation for the training data to re-label the noisy samples. We outperform existing methods on a new benchmark that consists of training on two large-scale noisy multi-label CXR datasets and testing on two clean multi-label CXR datasets. One drawback with SGVAL is that it does not account for imbalanced learning, which is an important topic when training with CXR datasets given that they generally present an imbalanced distribution of samples per class. Therefore, we plan to develop imbalanced learning approaches to improve the model optimisation on CXR datasets.

References

1. Ben-Cohen, A., Zamir, N., Ben-Baruch, E., Friedman, I., Zelnik-Manor, L.: Semantic diversity learning for zero-shot multi-label classification. In: Proceedings of the IEEE/CVF International Conference on Computer Vision. pp. 640–650 (2021)
2. Burges, C., Shaked, T., Renshaw, E., Lazier, A., Deeds, M., Hamilton, N., Hullender, G.: Learning to rank using gradient descent. In: Proceedings of the 22nd international conference on Machine learning. pp. 89–96 (2005)
3. Bustos, A., Pertusa, A., Salinas, J.M., de la Iglesia-Vayá, M.: Padchest: A large chest x-ray image dataset with multi-label annotated reports. *Medical image analysis* **66**, 101797 (2020)
4. Demner-Fushman, D., Kohli, M.D., Rosenman, M.B., Shooshan, S.E., Rodriguez, L., Antani, S., Thoma, G.R., McDonald, C.J.: Preparing a collection of radiology examinations for distribution and retrieval. *Journal of the American Medical Informatics Association* **23**(2), 304–310 (2016)
5. Goldberger, J., Ben-Reuven, E.: Training deep neural-networks using a noise adaptation layer (2016)
6. Han, B., Yao, Q., Yu, X., Niu, G., Xu, M., Hu, W., Tsang, I., Sugiyama, M.: Co-teaching: Robust training of deep neural networks with extremely noisy labels. *Advances in neural information processing systems* **31** (2018)
7. Hermoza, R., Maicas, G., Nascimento, J.C., Carneiro, G.: Region proposals for saliency map refinement for weakly-supervised disease localisation and classification. In: International Conference on Medical Image Computing and Computer-Assisted Intervention. pp. 539–549. Springer (2020)
8. Huang, G., Liu, Z., Van Der Maaten, L., Weinberger, K.Q.: Densely connected convolutional networks. In: Proceedings of the IEEE conference on computer vision and pattern recognition. pp. 4700–4708 (2017)
9. Huang, J., Qu, L., Jia, R., Zhao, B.: O2u-net: A simple noisy label detection approach for deep neural networks. In: Proceedings of the IEEE/CVF International Conference on Computer Vision. pp. 3326–3334 (2019)
10. Irvin, J., Rajpurkar, P., Ko, M., Yu, Y., Ciurea-Ilcus, S., Chute, C., Marklund, H., Haghighi, B., Ball, R., Shpanskaya, K., et al.: Chexpert: A large chest radiograph

- dataset with uncertainty labels and expert comparison. In: Proceedings of the AAAI conference on artificial intelligence. vol. 33, pp. 590–597 (2019)
11. Irvin, J., et al.: Chexpert: A large chest radiograph dataset with uncertainty labels and expert comparison. In: AAAI. vol. 33, pp. 590–597 (2019)
 12. Johnson, J., Douze, M., Jégou, H.: Billion-scale similarity search with GPUs. *IEEE Transactions on Big Data* **7**(3), 535–547 (2019)
 13. Kingma, D.P., Ba, J.: Adam: A method for stochastic optimization. *arXiv preprint arXiv:1412.6980* (2014)
 14. Lee, J., Yoon, W., Kim, S., Kim, D., Kim, S., So, C.H., Kang, J.: Biobert: a pre-trained biomedical language representation model for biomedical text mining. *Bioinformatics* **36**(4), 1234–1240 (2020)
 15. Li, J., Socher, R., Hoi, S.C.: Dividemix: Learning with noisy labels as semi-supervised learning. *arXiv preprint arXiv:2002.07394* (2020)
 16. Litjens, G., Kooi, T., Bejnordi, B.E., Setio, A.A.A., Ciompi, F., Ghafoorian, M., Van Der Laak, J.A., Van Ginneken, B., Sánchez, C.I.: A survey on deep learning in medical image analysis. *Medical image analysis* **42**, 60–88 (2017)
 17. Liu, F., Tian, Y., Chen, Y., Liu, Y., Belagiannis, V., Carneiro, G.: Acpl: Anti-curriculum pseudo-labelling for semi-supervised medical image classification. *arXiv preprint arXiv:2111.12918* (2021)
 18. Loshchilov, I., Hutter, F.: Sgdr: Stochastic gradient descent with warm restarts. *arXiv preprint arXiv:1608.03983* (2016)
 19. Ma, C., Wang, H., Hoi, S.C.: Multi-label thoracic disease image classification with cross-attention networks. In: *International Conference on Medical Image Computing and Computer-Assisted Intervention*. pp. 730–738. Springer (2019)
 20. Oakden-Rayner, L.: Exploring the chestxray14 dataset: problems. *Wordpress: Luke Oakden Rayner* (2017)
 21. Oakden-Rayner, L.: Exploring large-scale public medical image datasets. *Academic radiology* **27**(1), 106–112 (2020)
 22. Paszke, A., Gross, S., Massa, F., Lerer, A., Bradbury, J., Chanan, G., Killeen, T., Lin, Z., Gimelshein, N., Antiga, L., et al.: Pytorch: An imperative style, high-performance deep learning library. *Advances in neural information processing systems* **32** (2019)
 23. Rajpurkar, P., Irvin, J., Zhu, K., Yang, B., Mehta, H., Duan, T., Ding, D., Bagul, A., Langlotz, C., Shpanskaya, K., et al.: Chexnet: Radiologist-level pneumonia detection on chest x-rays with deep learning. *arXiv preprint arXiv:1711.05225* (2017)
 24. Russakovsky, O., Deng, J., Su, H., Krause, J., Satheesh, S., Ma, S., Huang, Z., Karpathy, A., Khosla, A., Bernstein, M., et al.: Imagenet large scale visual recognition challenge. *International journal of computer vision* **115**(3), 211–252 (2015)
 25. Wang, X., Peng, Y., Lu, L., Lu, Z., Bagheri, M., Summers, R.M.: Chestx-ray8: Hospital-scale chest x-ray database and benchmarks on weakly-supervised classification and localization of common thorax diseases. In: *Proceedings of the IEEE conference on computer vision and pattern recognition*. pp. 2097–2106 (2017)
 26. Xia, X., Liu, T., Han, B., Wang, N., Gong, M., Liu, H., Niu, G., Tao, D., Sugiyama, M.: Part-dependent label noise: Towards instance-dependent label noise. *Advances in Neural Information Processing Systems* **33**, 7597–7610 (2020)
 27. Yao, Y., Liu, T., Han, B., Gong, M., Deng, J., Niu, G., Sugiyama, M.: Dual t: Reducing estimation error for transition matrix in label-noise learning. *Advances in neural information processing systems* **33**, 7260–7271 (2020)
 28. Zhang, Y., Gong, B., Shah, M.: Fast zero-shot image tagging. In: *2016 IEEE Conference on Computer Vision and Pattern Recognition (CVPR)*. pp. 5985–5994. IEEE (2016)